Optical frequency comb interference profilometry using compressive sensing

Quang Duc Pham and Yoshio Hayasaki*

Center for Optical Research and Education (CORE), Utsunomiya University 7-1-2 Yoto, Utsunomiya 321-8585, Japan

**hayasaki@opt.utsunomiya-u.ac.jp*

Abstract: We describe a new optical system using an ultra-stable mode-locked frequency comb femtosecond laser and compressive sensing to measure an object's surface profile. The ultra-stable frequency comb laser was used to precisely measure an object with a large depth, over a wide dynamic range. The compressive sensing technique was able to obtain the spatial information of the object with two single-pixel fast photo-receivers, with no mechanical scanning and fewer measurements than the number of sampling points. An optical experiment was performed to verify the advantages of the proposed method.

©2013 Optical Society of America

OCIS codes: (100.3175) Interferometric imaging; (110.1758) Computational imaging; (110.6880) Three-dimensional image acquisition; (070.6120) Spatial light modulators; (120.3180) Interferometry.

References and links

1. J. C. Wyant, "Testing aspherics using two-wavelength holography," Appl. Opt. **10**(9), 2113–2118 (1971).
2. P. S. Lam, J. D. Gaskill, and J. C. Wyant, "Two-wavelength holographic interferometer," Appl. Opt. **23**(18), 3079–3081 (1984).
3. C. Wagner, W. Osten, and S. Seebacher, "Direct shape measurement by digital wavefront reconstruction and multiwavelength contouring," Opt. Eng. **39**(1), 79–85 (2000).
4. A. Wada, M. Kato, and Y. Ishii, "Multiple-wavelength digital holographic interferometry using tunable laser diodes," Appl. Opt. **47**(12), 2053–2060 (2008).
5. K. N. Joo and S. W. Kim, "Refractive index measurement by spectrally resolved interferometry using a femtosecond pulse laser," Opt. Lett. **32**(6), 647–649 (2007).
6. K. Minoshima, K. Arai, and H. Inaba, "Two-Color Interferometry using frequency combs for high-accuracy self-correction of air refractive index," Opt. Express **19**, 26095–26105 (2011).
7. C. E. Towers, D. P. Towers, D. T. Reid, W. N. MacPherson, R. R. J. Maier, and J. D. C. Jones, "Fiber interferometer for simultaneous multiwavelength phase measurement with a broadband femtosecond laser," Opt. Lett. **29**(23), 2722–2724 (2004).
8. J. S. Oh and S.-W. Kim, "Femtosecond laser pulses for surface-profile metrology," Opt. Lett. **30**(19), 2650–2652 (2005).
9. K. Körner, G. Pedrini, I. Alexeenko, T. Steinmetz, R. Holzwarth, and W. Osten, "Short temporal coherence digital holography with a femtosecond frequency comb laser for multi-level optical sectioning," Opt. Express **20**(7), 7237–7242 (2012).
10. S. Choi, M. Yamamoto, D. Moteki, T. Shioda, Y. Tanaka, and T. Kurokawa, "Frequency-comb-based interferometer for profilometry and tomography," Opt. Lett. **31**(13), 1976–1978 (2006).
11. P. Balling, P. Křen, P. Mašika, and S. A. van den Berg, "Femtosecond frequency comb based distance measurement in air," Opt. Express **17**(11), 9300–9313 (2009).
12. M. T. L. Hsu, I. C. M. Littler, D. A. Shaddock, J. Herrmann, R. B. Warrington, and M. B. Gray, "Subpicometer length measurement using heterodyne laser interferometry and all-digital rf phase meters," Opt. Lett. **35**(24), 4202–4204 (2010).
13. M. Cui, M. G. Zeitouny, N. Bhattacharya, S. A. van den Berg, and H. P. Urbach, "Long distance measurement with femtosecond pulses using a dispersive interferometer," Opt. Express **19**(7), 6549–6562 (2011).
14. J. Ye, "Absolute measurement of a long, arbitrary distance to less than an optical fringe," Opt. Lett. **29**(10), 1153–1155 (2004).
15. J. Lee, Y. J. Kim, K. Lee, S. Lee, and S. W. Kim, "Time-of-flight measurement with femtosecond light pulses," Nat. Photonics **4**(10), 716–720 (2010).
16. Y. Salvadé, N. Schuhler, S. Lévêque, and S. Le Floch, "High-accuracy absolute distance measurement using frequency comb referenced multiwavelength source," Appl. Opt. **47**(14), 2715–2720 (2008).
17. S. Yokoyama, T. Yokoyama, Y. Hagihara, T. Araki, and T. Yasui, "A distance meter using a terahertz intermode beat in an optical frequency comb," Opt. Express **17**(20), 17324–17337 (2009).

#189856 - $15.00 USD Received 1 May 2013; revised 12 Jul 2013; accepted 19 Jul 2013; published 2 Aug 2013

18. K. Minoshima and H. Matsumoto, "High-accuracy measurement of 240-m distance in an optical tunnel by use of a compact femtosecond laser," Appl. Opt. **39**(30), 5512–5517 (2000).
19. D. L. Donoho, "Compressed sensing," IEEE Trans. Inf. Theory **52**(4), 1289–1306 (2006).
20. E. J. Candès and T. Tao, "Near optimal signal recovery from random projections: Universal encoding strategies?" IEEE Trans. Inf. Theory **52**(12), 5406–5425 (2006).
21. M. F. Duarte, M. A. Davenport, D. Takhar, J. N. Laska, T. Sun, K. F. Kelly, and R. G. Baraniuk, "Single-pixel imaging via compressive sampling," IEEE Signal Process. Mag. **25**(2), 83–91 (2008).
22. W. Chan, K. Charan, D. Takhar, K. Kelly, R. Baraniuk, and D. Mittleman, "A Single-pixel terahertz imaging system based on compressed sensing," Appl. Phys. Lett. **93**(12), 121105 (2008).
23. D. J. Brady, K. Choi, D. L. Marks, R. Horisaki, and S. Lim, "Compressive holography," Opt. Express **17**(15), 13040–13049 (2009).
24. C. F. Cull, D. A. Wikner, J. N. Mait, M. Mattheiss, and D. J. Brady, "Millimeter-wave compressive holography," Appl. Opt. **49**(19), E67–E82 (2010).
25. R. Berinde, P. Indyk, and M. Ruzic, "Practical near-optimal sparse recovery in the L1 norm," Communication, Control, and Computing, 2008 46th Annual Allerton Conference, 198–205, 23–26 Sept. (2008).
26. E. J. Candès and J. Romberg, "Signal recovery from random projections," in Computational Imaging III, Proc. SPIE Conf. 5674, 76–86, 31 March. (2005).

1. Introduction

In many industrial applications, it is important to determine the surface profile of an object having a large depth, and the demand for rapid and high-accuracy surface profile observation is growing day by day. Traditional optical interferometry is known to have high axial resolution, but an inherent problem with this technique is a 2π phase ambiguity that occurs when the illuminated surface has a height difference larger than the wavelength [1,2]. In this method, the modulo-2π phase distribution must be unwrapped to reconstruct the three-dimensional (3D) shape of the object [1,2]. Another approach is multiple-wavelength method, which uses more than two illumination wavelengths to overcome the 2π ambiguity of two-wavelength method [3,4]. Although two-wavelength and multi-wavelength interferometry can widen the dynamic measurement range from a few micrometers to several millimeters, the measurement range depends on the number of synthetic wavelengths and the characteristics of the light sources [4]. Although the dynamic range can be expanded, the system becomes very complex and is not appropriate for general-purpose profilometry.

Recently developed optical mode-locked frequency comb femtosecond lasers have been exploited in many applications due to their many useful properties. By using a frequency comb femtosecond laser, the refractive index and thickness can be determined by using spectrally resolved single- [5] or two-color interferometry [6], and phase measurement [7], profilometry, and tomography of the objects can also be carried out by sweeping the comb interval frequency and using scanning interferometry [8–10]. In particular, by employing an optical mode-locked frequency comb femtosecond laser, high-precision, wide-dynamic-range absolute distance measurement can be achieved with various methods, including coherence interferometry [11–13], time-of-flight measurements [14,15], a combination of coherence interferometry and time-of-flight measurements [14], intermode beat modification of the optical frequency comb [16,17], and a method exploiting the radio-frequency domain of a frequency comb femtosecond laser [18]. Technical speaking, the object's profile can be absolutely specified by measuring the distance of all object points, but it will be very time consuming and the accuracy is limited by the need to mechanically scan.

Additionally, compressive sensing (CS) is a new digital signal processing technique designed to acquire and recover a physical signal from relatively few measurements with potentially high resolution [19,20]. CS involves the original idea of using a combination of sparse representation and pseudorandom sampling, which enables CS to be applied to extract the maximum amount of signal information from the minimum amount of measurements. CS can be used to compress data in digital image processing with an efficiency proven to be much better than conventional techniques like JPEG and JPEG 2000. Recently, using CS, a single-pixel camera [21] and a single-pixel terahertz imaging system [22] have been realized by measuring inner products between the scene and a set of random test functions. This data acquisition process has been shown to be more efficient than the sampling scheme used in conventional sensing methods, because redundant data is not sampled [21,22]. Moreover,

#189856 - $15.00 USD Received 1 May 2013; revised 12 Jul 2013; accepted 19 Jul 2013; published 2 Aug 2013
(C) 2013 OSA

Gabor holography recording process has been employed and proved to work as a compressive encoder in spatial frequency domain, thus, the CS technique is also able to be applied to reconstruct the 3D tomography from a single 2D optical monochromatic digital holography [23] and millimeter wave digitized holography [24].

In this paper, we propose a new optical profile measurement system that has a high dynamic range implemented with a frequency comb femtosecond laser based on the CS technique to perform a spatial measurement. The frequency comb femtosecond laser has an extreme stable optical frequency modes, it enabled to record the phase information of the interference signal of all the points on the object's surface very precisely. The CS technique was carried out by encoding an object wave using a spatial light modulator (SLM), which allows the entire object surface to be reconstructed from fewer measurements than the number of sampling points [25,26]. We demonstrate the idea and its advantages experimentally.

2. Principle

2.1 Interference imaging with optical mode-locked frequency comb femtosecond laser

In the frequency domain, a mode-locked frequency comb femtosecond laser can be regarded as many separate monochromatic light sources with extremely long coherence length. Denoting the repeat and offset frequencies of the light sources as f_R and f_O, respectively, the harmonic frequency of order n is given by $f_n = f_O + nf_R$, where $0 \le n \le N_{max}$ and N_{max} is the maximum harmonic frequency order of the frequency comb laser.

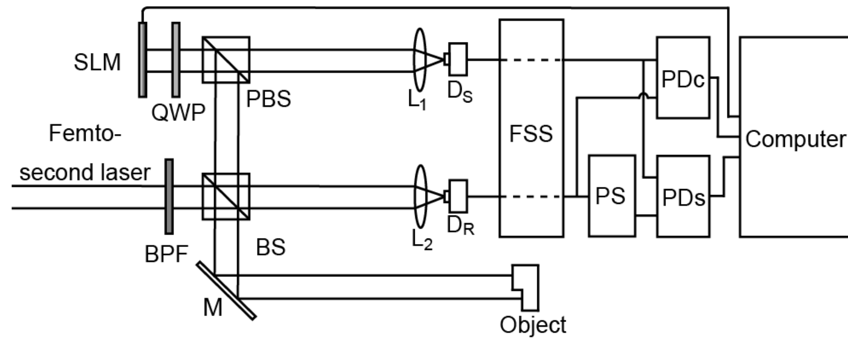

Fig. 1. Experimental setup. BPF, band pass filter; BS, beam splitter; PBS, polarization beam splitter; M, reflecting mirror; L, lens; SLM, spatial light modulator; QWP, quarter wave plate; D_S, D_R, fast photo-receivers; FSS, frequency selection system; PD_C, PD_S, phase detectors; M, mirror; PS, phase shifter.

For the optical setup shown in Fig. 1, the object wave of a specific frequency of the light source, when reflected from an object point, is expressed by $A_n(x, y)\exp\{-j[w_n t + \varphi_n(x, y)]\}$, where x and y indicate the position of the point, $w_n = 2\pi f_n$ is the angular frequency, and φ_n is the phase of the object point. When the object wave is reflected from the SLM, it is modulated with a modulation function $R_n(x,y,l)$ and is then focused on the sensor of the fast photo-receiver D_S at the focal point of the lens L_1. The interference pattern of all the points on the object surface is expressed by

$$U_n(t) = \sum_{y=1}^{Y}\sum_{x=1}^{X} R_n(x, y, l) A_n(x, y) e^{-j[w_n t + \varphi_n(x,y)]}, \tag{1}$$

where X and Y are related to the observed area and expressed in units of pixels, and $l > 0$ indicates the measurement order.

The light source is a comb frequency laser with a maximum harmonic frequency order of N_{max}; therefore, the interference pattern in the sensor image is the summation of the monochromatic interference patterns of all optical frequencies, expressed by

#189856 - $15.00 USD Received 1 May 2013; revised 12 Jul 2013; accepted 19 Jul 2013; published 2 Aug 2013
(C) 2013 OSA

$$U_{TT}(t) = \sum_{n=1}^{N_{\max}} U_n(x, y, t). \tag{2}$$

The interference pattern is sampled by D_S with a maximum response sampling frequency of f_{smax}. Suppose that the harmonic frequency order N closest to f_{smax} satisfies the condition $f_N \leq f_{smax} < f_{N+1}$.This means that the high-frequency component of $U_{TT}(t)$ will be cut-off after passing through D_S. The signal output from D_S is now rewritten in the form

$$U_{TN}(t) = \sum_{n=1}^{N} U_n(x, y, t). \tag{3}$$

Similarly, the signal passing through D_R is simply described by

$$U_{RTN}(t) = \sum_{n=1}^{N} A_{Rn} e^{-j(w_n t + \varphi_{Rn})}. \tag{4}$$

The output signals from D_S and D_R are led into a frequency selectable system (FSS) [23]. Only the sampled optical waves which with the frequency f_k corresponding to the harmonic frequency order k ($0 < k \leq N$) satisfies the condition of the FSS are passed through. Equations (3) and (4) are rewritten as

$$U_T(t) = \sum_{y=1}^{Y} \sum_{x=1}^{X} R_k(x, y, l) A_k(x, y) e^{-j[w_k t + \varphi_k(x, y)]} \tag{5}$$

and $U_{RT}(t) = A_{Rk} exp[-j(w_k t + \varphi_{Rk})]$, respectively. $U_T(t)$ and U_{RT}(t) are each separated into two components to measure the phases, as shown in Fig. 1. The output signal from phase-detector PD_C is described by

$$\begin{aligned} P_c(l) &= real[U^*_{RT}(t)]real[U_T(t)] \\ &= \sum_{y=1}^{Y} \sum_{x=1}^{X} \alpha R_k(x, y, l) A_{Rk} A_k(x, y) \{\cos[\Delta\varphi_k(x, y)] + \cos[2w_k t + \varphi_k(x, y) + \varphi_{Rk}]\}, \end{aligned} \tag{6}$$

where $U_{RT}*(t)$ is $U_{RT}(t)$ with the phase inverted because of characteristics of the phase detector, $\Delta\varphi_k(x,y) = \varphi_k(x,y) - \varphi_{Rk}$ is the phase difference between the coded object wave and the reference wave, and constant α characterizes the effect of the power splitter and the relation between the amplitudes of the output and input signals of the phase detector. The high-frequency component in Eq. (6) will be filtered by a low pass filter; thus, the output signal from the phase detector is simply described by

$$P_c(l) = \sum_{y=1}^{Y} \sum_{x=1}^{X} R_k(x, y, l) E_{ck}(x, y), \tag{7}$$

where $E_{ck}(x,y) = \alpha A_{RK} A_K(x,y)\cos[\Delta\varphi_k(x,y)]$. Before being led into the phase-detector PD_S, the phase of the reference wave is shifted by $\pi/2$ by a phase shifter (PS), and the output signal from the phase detector is expressed by

$$P_s(l) = \sum_{y=1}^{Y} \sum_{x=1}^{X} R_k(x, y, l) E_{sk}(x, y), \tag{8}$$

where $E_{sk}(x,y) = \beta A_{RK} A_K(x,y)\sin[\Delta\varphi_k(x,y)]$, and β is a different constant from α because of the attenuation caused by the phase shifter. When $E_{ck}(x,y)$ and $E_{sk}(x,y)$ are specified, $\Delta\varphi_k(x,y)$ is easily obtained by the following equation,

#189856 - $15.00 USD Received 1 May 2013; revised 12 Jul 2013; accepted 19 Jul 2013; published 2 Aug 2013
(C) 2013 OSA

$$\Delta\varphi_k(x,y) = \arctan[\frac{E_{sk}(x,y)}{E_{ck}(x,y)} \times \frac{\beta}{\alpha}]. \quad (9)$$

The depth difference $\Delta D(x,y)$ between the object and reference points is calculated by

$$\Delta D(x,y) = \frac{c[2\pi p + \Delta\varphi_k(x,y)]}{4\pi f_k n_g}, \quad (10)$$

where p is the integer part of the phase difference, c is the velocity of light, and n_g is the group refractive index of the medium. If the object depth is assumed to be smaller than half the wavelength of the waves selected by the FSS, then $p = 0$, and thus, the object profile can be specified without any 2π ambiguity.

2.2 Applying compressive sensing

The CS technique can be used to scan object information with a number of measurements fewer than the number of sampling points. In practice, however, CS is advantageous only for sparse signals [19, 20], which is not the case with an actual object. Therefore, instead of directly measuring the object profile, it can be obtained via an equivalent representation model that has sparse elements. First, a mask $R_k(x,y,l)$ is constructed by a pseudorandom pattern consisting of random binary elements of a Bernoulli matrix. Elements "0" and "1" correspond to two states, which block or pass light; the number of "1" and "0" elements in each pseudorandom pattern is the same. For each pseudorandom pattern $R_k(x,y,l)$, a shifted version denoted by $R_{sk}(x,y,l)$ is also generated as follows:

$$\begin{cases} R_{sk}(x,y,l) = 0 \text{ if } x = 1 \text{ and } y = 1 \\ R_{sk}(x,y,l) = R_k(X, y-1, l) \text{ if } x = 1 \text{ and } y > 1. \\ R_{sk}(x,y,l) = R_k(x-1, y, l) \text{ if } x > 1 \end{cases} \quad (11)$$

From Eqs. (7) and (8), when the shifted version of $R_k(x,y,l)$ is displayed on the SLM, the outputs from PD_C and PD_S are expressed by

$$P_{sc}(l) = \sum_{y=1}^{Y}\sum_{x=1}^{X} R_{sk}(x,y,l)E_{ck}(x,y), \quad (12)$$

$$P_{ss}(l) = \sum_{y=1}^{Y}\sum_{x=1}^{X} R_{sk}(x,y,l)E_{sk}(x,y). \quad (13)$$

From Eqs. (7) and (12), the difference $\Delta P_c(l)$ obtained by subtracting $P_{cs}(l)$ from $P_c(l)$ is

$$\Delta P_c(l) = \sum_{y=1}^{Y}\sum_{x=1}^{X} R_k(x,y,l)\Delta E_{ck}(x,y), \quad (14)$$

where

$$\begin{cases} \Delta E_{ck}(x,y) = E_{ck}(x,y) - E_{ck}(x+1,y) \\ \Delta E_{ck}(x,y) = E_{ck}(x,y) - E_{ck}(1,y+1) \text{ if } x = X. \\ \Delta E_{ck}(x,y) = E_{ck}(x,y) \text{ if } x = X \text{ and } y = Y \end{cases} \quad (15)$$

Similarly, from Eqs. (8) and (13), the difference $\Delta P_s(l)$ obtained by subtracting $P_{ss}(l)$ from $P_s(l)$ is

$$\Delta P_s(l) = \sum_{y=1}^{Y}\sum_{x=1}^{X} R_k(x,y,l)\Delta E_{sk}(x,y), \quad (16)$$

#189856 - $15.00 USD Received 1 May 2013; revised 12 Jul 2013; accepted 19 Jul 2013; published 2 Aug 2013
(C) 2013 OSA

where

$$\begin{cases} \Delta E_{sk}(x,y) = E_{sk}(x,y) - E_{sk}(x+1,y) \\ \Delta E_{sk}(x,y) = E_{sk}(x,y) - E_{sk}(1,y+1) \text{ if } x = X \\ \Delta E_{sk}(x,y) = E_{sk}(x,y) \text{ if } x = X \text{ and } y = Y \end{cases}. \tag{17}$$

From Eqs. (15) and (17), it can be seen that $\Delta E_{ck}(x,y)$ and $\Delta E_{sk}(x,y)$ are equivalent representation models of $E_{ck}(x,y)$ and $E_{sk}(x,y)$, respectively. Because the consecutive points in a line on the object often have similar depth and intensity, on some areas of the object, $\Delta E_{ck}(x,y)$ and $\Delta E_{sk}(x,y)$ are approximately equal to 0. This means that $\Delta E_{ck}(x,y)$ and $\Delta E_{sk}(x,y)$ can be considered as sparse signals which can be obtained and reconstructed by CS [19, 20].

It is assumed that $\Delta E_{ck}(x,y)$ and $\Delta E_{sk}(x,y)$ are the same m-sparse signal, and thus the minimum number of measurements required to exactly reconstruct the original signal is calculated by

$$M = O(2m\log(XY/m)). \tag{18}$$

This equation is also considered as a condition of CS [19, 20]. When M pseudorandom patterns of $R_k(x,y,l)$ and $R_{ks}(x,y,l)$ are used, from Eqs. (14) and (16), the measurement process can be described by the equations

$$\Delta P_c = \Phi_R \Delta E_c, \tag{19}$$

and

$$\Delta P_s = \Phi_R \Delta E_s, \tag{20}$$

where ΔP_c and ΔP_s are $M \times 1$ column vectors of measurements, ΔE_c and ΔE_s are column vectors with $X \times Y$ pixels of $\Delta E_{ck}(x,y)$ and $\Delta E_{sk}(x,y)$ ordered in an $XY \times 1$ vector, and the measurement matrix Φ_R is $M \times XY$.

In order to reconstruct sparse signals of $\Delta E_{ck}(x,y)$ and $\Delta E_{sk}(x,y)$, the $l1$ minimization method is selected. It is summarized by [25, 26]:

$$\min \| \Delta E_c \|_{l1} \text{ subject to } \| \Phi_R \Delta E_c - \Delta P_c \|_2 \le \varepsilon, \tag{21}$$

$$\min \| \Delta E_s \|_{l1} \text{ subject to } \| \Phi_R \Delta E_s - \Delta P_s \|_2 \le \varepsilon, \tag{22}$$

where ε is a tolerance that determines the accuracy of the reconstructed signal [19, 20]. When all values of $\Delta E_c(x,y)$ and $\Delta E_s(x,y)$ are specified by the reconstruction process in Eqs. (21) and (22), $E_{ck}(x,y)$ and $E_{sk}(x,y)$ are calculated by Eqs. (15) and (17), so that the profile of the object is measured by applying Eqs. (9) and (10).

3. Experiment

The experimental setup is shown in Fig. 1. A frequency comb femtosecond laser (FEMTOSOURCE rainbow, FEMTOLASERS, Inc.) with a repetition rate of 76 MHz was used. The object and reference waves were sampled by two photo-receivers with a maximum frequency response of 1 Ghz. The FSS was designed to select the 13th frequency harmonic corresponding to the frequency of 988 MHz of the light source, to allow an object with a depth smaller than 15.18 cm to be detected without any 2π ambiguity. The attenuation caused by the phase shifter, expressed by $\beta/\alpha = 0.8$, was measured from the ratio between the amplitudes of the input and output signals of the phase shifter.

Three kinds of pseudorandom pattern with 4 × 4, 6 × 6, and 10 × 10 random binary elements, as shown in Figs. 2(a)-2(f), were used to encode the object wave. The SLM pixel size was 26 μm. Each binary element of the 4 × 4, 6 × 6, and 10 × 10 pseudorandom patterns was constructed with 60 × 60, 40 × 40, and 24 × 24 pixels of the SLM, respectively, and the scanning range in this case was 6.24 mm × 6.24 mm.

#189856 - $15.00 USD Received 1 May 2013; revised 12 Jul 2013; accepted 19 Jul 2013; published 2 Aug 2013
(C) 2013 OSA

In the first experiment, a plane mirror was used as the target object to evaluate the stability of the system and the accuracy of the proposed method. For each pseudorandom pattern displayed on the SLM, 5000 samples of the phase information were measured by the phase detector system at intervals of 100 μs. The phase information corresponding to the displayed pseudorandom pattern was the average value calculated from 5000 measured ones. In order to precisely reconstruct the object's profile, the number of measurements should be not smaller than the theoretical one calculated by Eq. (18). Considering the object's structure, 12 measurements with 4 × 4 and 6 × 6 pseudorandom patterns and 40 measurements with 10 × 10 pseudorandom patterns were performed to reconstruct the equivalent representation model of the object by Eqs. (21) and (22), then Eqs. (15) and (17) were applied to obtain the object's profile. The results were shown in Figs. 3(a)-3(c).

In fact, it is very difficult to exactly know the sparse number of an actual object, thus, the profile of the object reconstructed from different numbers of measurements was to evaluate the error of the system. For each number of measurements, an object profile was reconstructed by Eqs. (21), (22), (15) and (17), the corresponding accuracy was evaluated by calculating the root mean square (RMS) error. In this case, because the original object was considered to be a perfect flat plane, the RMS error was simply calculated from all measured points and their average depth. The result is shown in Fig. 4.

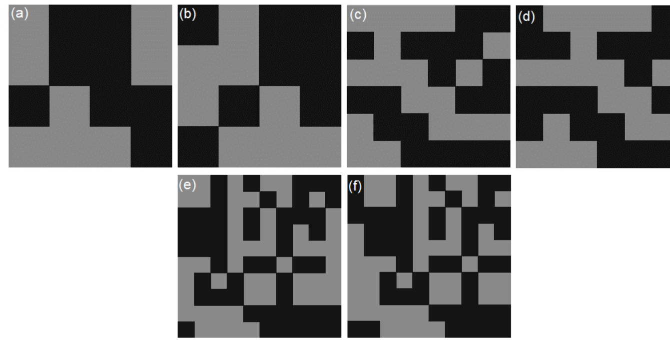

Fig. 2. Pseudorandom patterns of (a) 4 × 4 elements and (b) the corresponding shifted version, (c) 6 × 6 elements and (d) the corresponding shifted version, and (e) 10 × 10 elements and (f) the corresponding shifted version used to encode the object wave.

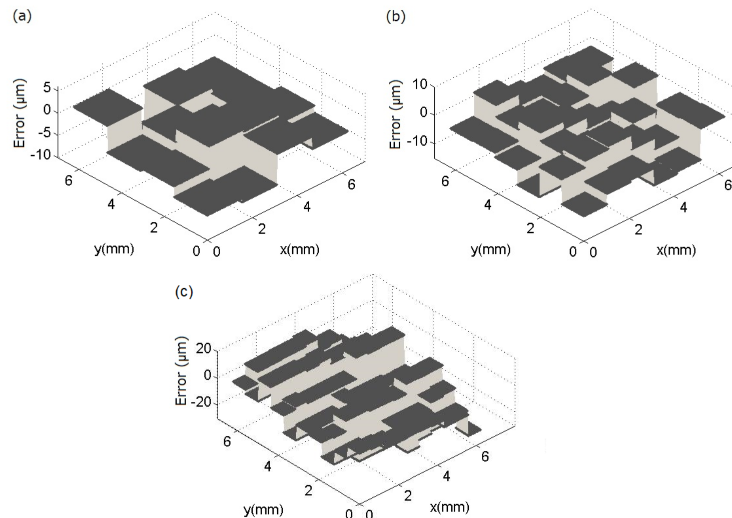

Fig. 3. The accuracy of the proposed method, measured with (a) 4 × 4, (b) 6 × 6 and (c) 10 × 10 pseudorandom patterns.

#189856 - $15.00 USD Received 1 May 2013; revised 12 Jul 2013; accepted 19 Jul 2013; published 2 Aug 2013
(C) 2013 OSA

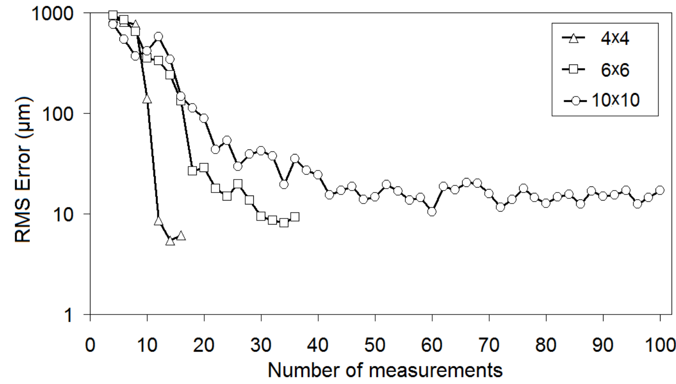

Fig. 4. The accuracy of the proposed method with different types of pseudorandom patterns was investigated.

In the second experiment, two flat mirrors located in different planes 4 cm apart were used as the target object. The same process as in the first experiment was applied. The object profile shown in Fig. 5(a) was reconstructed from 12 measurements with 4 × 4 pseudorandom patterns. Another object constructed of three flat mirrors located in different planes, where the distance between the first and second ones was about 30 mm, and the distance between the first and third ones was about 50 mm, was also measured. The profile, which was obtained by 26 measurements of 6 × 6 pseudorandom patterns, is shown in Fig. 5(b).

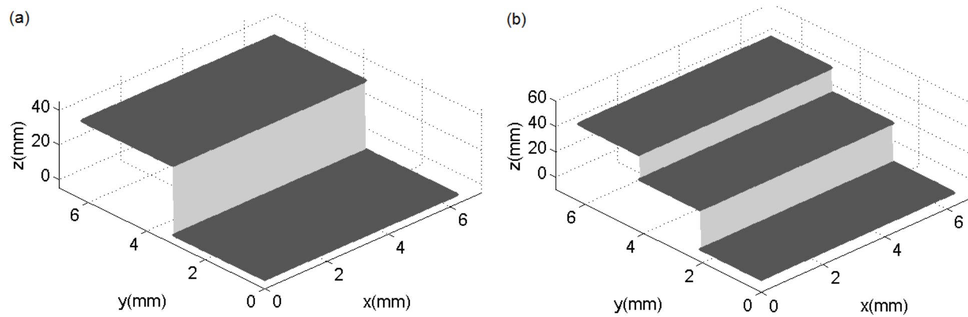

Fig. 5. Actual object profiles measured with (a) 4 × 4 and (b) 6 × 6 pseudorandom patterns.

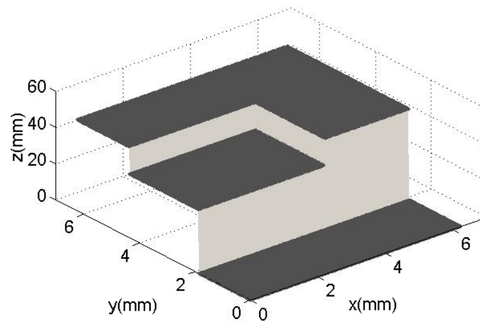

Fig. 6. Actual object profile measured with 10 × 10 pseudorandom patterns.

Finally, a more complicated object constructed of three flat mirrors located in different planes, where the distance between the first and second ones was about 30 mm, and the difference between the first and third ones was about 50 mm, was also measured. The profile, which was obtained by 80 measurements of 10 × 10 pseudorandom patterns, is shown in Fig. 6.

#189856 - $15.00 USD Received 1 May 2013; revised 12 Jul 2013; accepted 19 Jul 2013; published 2 Aug 2013
(C) 2013 OSA

4. Conclusions

We have proposed a new method for measuring an object's profile with an ultra-stable mode-locked frequency comb femtosecond laser. A theoretical analysis was described for explaining the operating principle of the system, for examining the performance, for learning about the requirements of the devices for implementation, and for visualizing the experimental results of the proposed system. Use of the ultra-stable mode-locked frequency comb femtosecond laser ensures high accuracy of each measurement. The CS technique allows scanning and reconstruction of the object profile with fewer measurements than the number of object points. The experimental results demonstrated the feasibility and advantages of the proposed method. The scanning range depended on the size of the SLM. The scanning resolution can be easily changed, and the maximum achievable resolution can be as high as the resolution of the SLM.

The accuracy was dependent on the number of measurements, but when the number of measurements was greater than that required by the CS conditions, the RMS error was considered to be constant. For more complicated objects, a random mask with smaller pixel size was required to be used.

In the experiment, the object profile was measured with a single-color setup. If a two-color setup is used [18], an object with much larger depth can be measured.

This system did not require any mechanical scanning, and therefore, errors related to mechanical devices could be eliminated. However, the accuracy of the system was limited because of the low contrast of the SLM and the low sensitivity of the phase detectors. Finally, when the more sensitive fast photo-receivers are used, the low intensity of the scattering light of the object can be obtained so that the proposed method can be applied for profilometry of an actual object.